NUCL SCI TECH (2020) 31:103
https://doi.org/10.1007/s41365-020-00808-4

Train probe for beam diagnostics of the SC200 superconducting cyclotron

Le-Xing Hu[1,2] · Kai-Zhong Ding[1] · Yun-Tao Song[1] · Yu-Cheng Wu[3] · Kai Yao[3]

Received: 10 June 2020 / Revised: 7 September 2020 / Accepted: 9 September 2020 / Published online: 12 October 2020

Abstract The SC200 proton therapy system commissioned by the Hefei CAS Ion Medical and Technical Devices Co., Ltd. (HFCIM; Hefei, China) and the Joint Institute for Nuclear Research (JINR; Dubna, Russia) has made significant progress. A main radial beam diagnostic system (MRBDS) equipped with a new type of train probe was developed to satisfy the requirements of beam diagnosis. In this paper, the detailed design of the mechanical structure and electronics system of the MRBDS is presented. The electronics system, which includes hardware and software components, was tested and calibrated. The results show that measurement errors can be significantly reduced by the designed calibration procedures. The repeatability of the mechanical structure was also verified, and the experimental results indicate that the unidirectional repeatability of the positioning is better than 0.3 mm. Finally, the MRBDS was used to measure the phase lag of the particles in the beam, and the results showed a high degree of agreement with theoretical calculations, which proved the applicability and high efficiency of the MRBDS.

This work was supported by the funding of the CN-RU cooperation cyclotron design (No. 1604b0602005).

✉ Kai-Zhong Ding
kzding@ipp.ac.cn

1 Institute of Plasma Physics, Chinese Academy of Sciences, Hefei 230031, China

2 University of Science and Technology of China, Hefei 230026, China

3 Hefei CAS Ion Medical and Technical Devices Co., Ltd, Hefei 230088, China

Keywords Train probe · Beam diagnostic · Cyclotron · Measurement and calibration · Commissioning

1 Introduction

Malignant tumors are one of the major diseases threatening human health and life [1–3]. Proton therapy has become an important and widely employed cancer treatment technology owing to its remarkable efficiency and minor side effects. The SC200 superconducting cyclotron, installed at the Hefei CAS Ion Medical and Technical Devices Co., Ltd. (HFCIM), can provide proton acceleration up to 200 MeV with a maximum beam current of $\sim$ 1 μA [4–7]. It is designed for tumor therapy with adjustable beam intensity, strong magnetic field, and high radio frequency (RF) interference. As an important part of the accelerator, the beam diagnostic system can provide critical information for beam diagnosis, which is crucial in beam tuning, key parameter optimization, and operation monitoring [8, 9].

The radial probe is the main diagnostic instrument for beam tuning and beam commissioning inside the cyclotron [10–12]. Roy et al. [13] developed a radial probe by chaining several carts end-to-end using hinged joints, which can move along the slotted track; however, it can be dislodged on the track. In addition, Acerbi et al. [14, 15] reported a movable multi-head probe equipped at the Milan K800 cyclotron whose movement was provided by a train. The absolute position of the probe was measured using marks on the rails, which were detected by the photoelectric sensor. However, the marks on the rails can be damaged by wear or particle bombardment. In addition, the application of photoelectric sensors and signal cables inside the cyclotron is not recommended because of the high vacuum environment.

The main radial beam diagnostic system (MRBDS) equipped with a new type of train probe has been developed to remain function under strong magnetic fields, high electromagnetic interference, and to adopt to the limited space of the cyclotron. The MRBDS can realize the measurement of beam intensity and position, thus achieving better positioning repeatability and higher reliability compared with previous designs. The MRBDS is composed of a mechanical structure and an electronics system, and the detailed design of each subassembly is described in the following sections.

The rest of this paper is organized as follows. Section 2 describes the detailed design of the MRBDS. In Sect. 3, the calibration and background noise tests of the measurement unit, as well as repeatability tests on the positioning of the train probe, are introduced. The MRBDS used to measure the phase lag of particles is described in Sect. 4. Finally, the conclusions are drawn in Sect. 5.

2 System design

2.1 Structural design

The mechanical structure of the MRBDS was developed to be compatible with the characteristics of the SC200. The design of the train probe enables the MRBDS to measure beam parameters from the central region to the extraction region of the cyclotron. The mechanical structure, shown in Fig. 1a, consists of a train probe module, railway module, drive module, vacuum module, and support base. To achieve suitable magnetic permeability and mechanical behaviors, stainless steel (SUS 316L) and copper were used as the main materials. The relative permeability of the materials is not allowed to exceed 1.05 to prevent the disturbance of the magnetic field distribution of the isochronous field.

The layout of the SC200 is shown in Fig. 2. The gap between the upper and lower poles of the SC200 is only 26.8 mm, which is too small for the radial probe to access. Additionally, the large spiral angle of up to 40° of the sectors [7, 16] also prevents the application of linear radial probes. Therefore, a new type of train probe moving along the curved guide rail was designed to be suitable for the limited space inside the cyclotron. The curved guide rail, which extends from the central region to the extraction region of the cyclotron, is mounted in the valley of the cyclotron across the median plane.

The train probe module, shown in Fig. 1b, is composed of nine carts and a long transmission rod. All carts are chained with link blocks using hinge pins, while each cart is clamped to the railway by two pairs of guide wheels at the bottom. A sectional view of the cart and railway is shown in Fig. 1c.

Small ceramic bearings were used to withstand the vacuum and high magnetic field environment inside the cyclotron. Each wheel fits tightly with the outer race of the two ceramic bearings that are installed coaxially to prevent wheel shaking. The inner race of the bearing is fitted with an eccentric bolt that can be adjusted with torque screwdrivers. The eccentric bolts are designed to adjust the tightness between the wheels and the guide rail, to improve the accuracy of the train probe movement and thus, measurement repeatability, in the case of severe wear on the wheels and guide rails.

A typical probe structure, shown in Fig. 1b, is composed of three electrically isolated tungsten fingers and a vertical wire. The former measures the axial distribution of the beam, and the latter provides information on the radial distribution of the beam [11, 13]. The differential fingers of the probe can be rotated to maintain their alignment perpendicular to the beam. The fingers and insulating blocks are clamped by the shield plates, which are designed to shield electromagnetic interference from the RF system. The side shield plates of the probe shown in Fig. 1b are not shown to illustrate the internal structure of the probe.

The vacuum module is composed of a long bellow, gate valve, exchange box, and related accessories. The drive module consists of a servo electric cylinder and feedback components. The screw stroke is approximately 2 m and enables the probe to be drawn completely outside the gate valve, such that the change or maintenance of the probe can be performed in the exchange box without breaking the cyclotron vacuum. A servo motor is used as the execution motor to ensure motion stability and kinematic accuracy. An absolute grating ruler is used to obtain the actual motion displacement of the probe and to realize closed-loop feedback to improve the positioning accuracy of the train probe.

2.2 Electronics system design

The beam diagnosis is based on the accurate measurement of the beam parameters and on the highly precise positioning of the probe. The probe mounted at the front end of the train converts the intensity signals of the beam into current signals. The electronics system provides beam intensity measurement and motion control of the train probe.

The hardware architecture of the electronics system is shown in Fig. 3a. It is composed of a beam measurement unit, transmission unit, and control unit. Picoammeters were used to achieve direct high-precision measurement of beam current signals, which can perform current–voltage

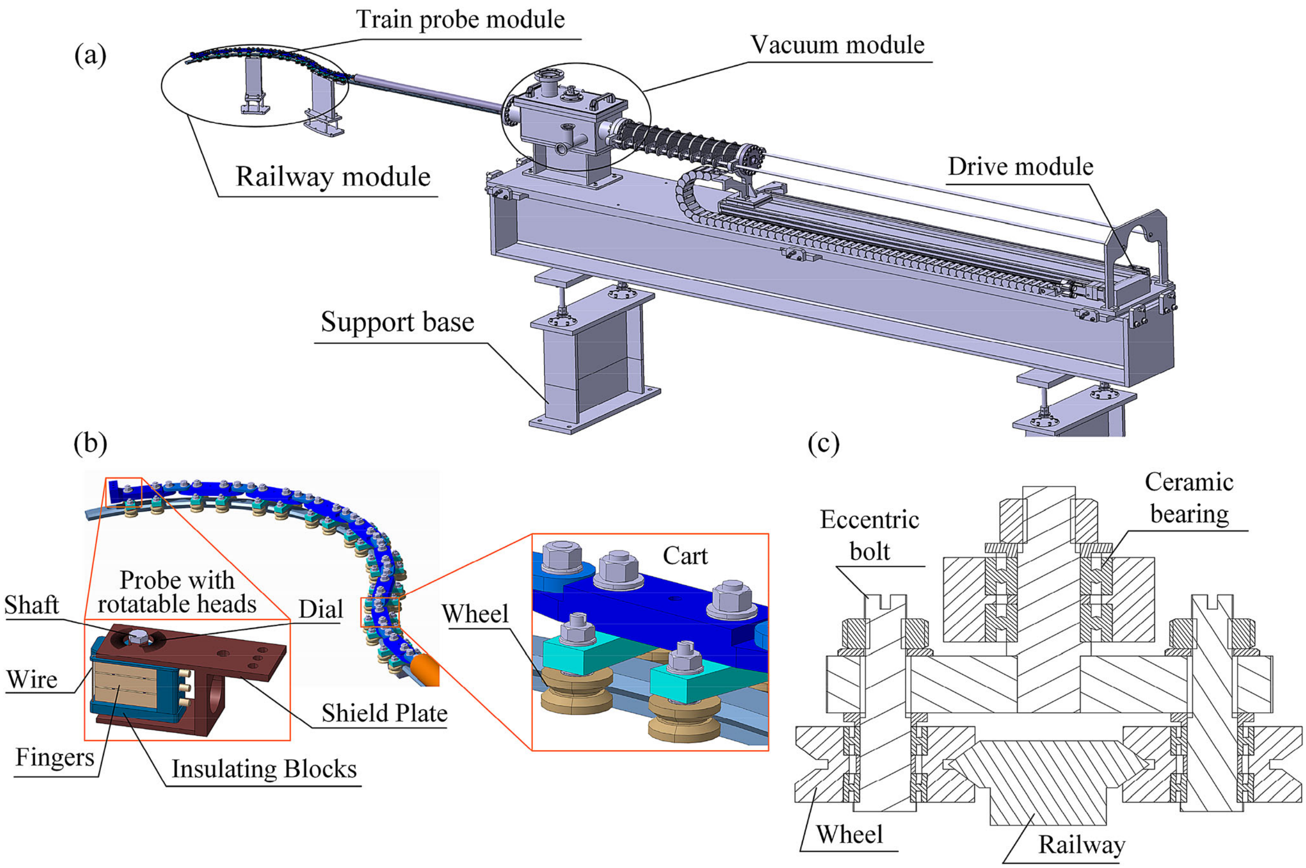

Fig. 1 (Color online) **a** Schematics of the mechanical structure. **b** Detailed drawing of the train probe module. **c** Sectional view of the train and railway

(I/V) conversion and can output analog voltage signals of $\pm$ 2 V in reverse. Therefore, the beam intensity can be obtained by measuring the analog voltage signal output by picoammeters using an acquisition card. A serial server was used for the network access to the serial ports of the picoammeters for integrated communication and real-time data monitoring. Owing to its high speed and high performance, Ethernet for Control Automation Technology (EtherCAT) was used as the communication protocol between the servo driver and the CompactRIO real-time controller. The CompactRIO controller was used to realize integrated control of the data acquisition, motion control, and communication with the accelerator control system (ACS). For the communication between the ACS and the CompactRIO controller, the OPC Unified Architecture (UA) technology was employed. The OPC UA communication protocol is a new data communication technology released by the OPC Foundation [17] and, as a cross-platform communication mode, it can eliminate the dependency on Windows OS with higher security and reliability.

Shielded twisted pair cables with polyimide insulation layers were used to deliver signals from the probe to withstand the high electromagnetic interference and vacuum environment inside the cyclotron. The shielded twisted pair cables are sufficiently flexible to move with the train probe along the curved guide rail. The application of single-ended grounding is recommended for the shielding layer of the shielded twisted pair cables, which can eliminate interference from the ground loops. The beam current signals were transmitted outside the cyclotron through electric feedthroughs. The feedthroughs and picoammeters were connected by coaxial cables. Specifically, all signal cables from the probe to the picoammeters are required to be properly shielded.

To reduce current leakage, appropriate insulation between different differential fingers and between differential fingers and the ground is required. Experimental tests show that the insulation resistance between the differential fingers or the ground is required to be greater than 100 MΩ. In addition, electromagnetic interference (EMI) power-line filters can filter harmonics higher than 50 Hz in the power grid and can prevent EMI coupling into the power grid. Therefore, suitable EMI filters were applied to improve the electromagnetic compatibility of the beam diagnostic electronics system.

Fig. 2 Layout of the SC200

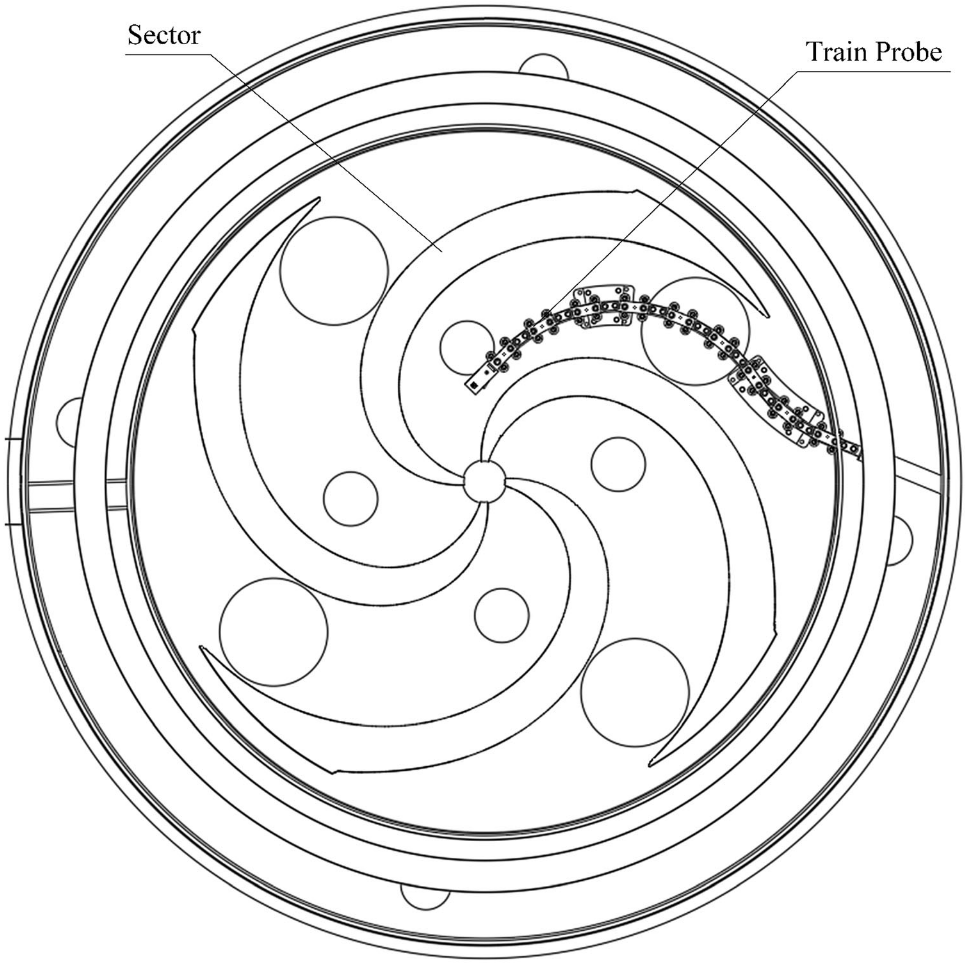

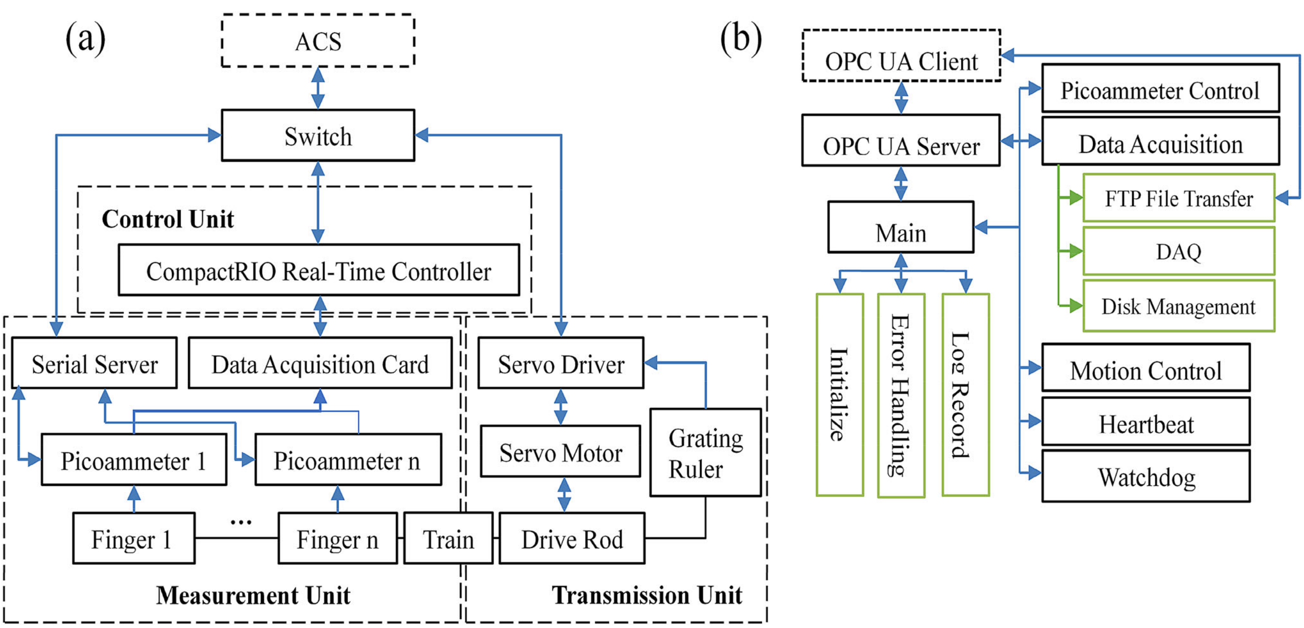

Fig. 3 **a** Hardware architecture of the electronics system. **b** Schematic diagram of the software architecture of the electronics system

The software component of the electronics system, shown in Fig. 3b, is composed of several modules, such as a main module, picoammeter control module, data acquisition module, and motion control module. Each module realizes the corresponding functions and achieves interconnected communication between the modules. The connection of different modules is shown in Fig. 3b.

The picoammeter control module controls the picoammeters and obtains current measurements. The motion control module realizes the motion control of the servo motor and the positioning of the probe. The OPC UA communication module provides communication between the beam diagnostic electronics system and the ACS to realize the control and monitoring of key parameters of the MRBDS. The data acquisition module realizes the fast acquisition of the analog voltage signal outputs by the picoammeters and provides data processing, file transfer via an FTP protocol, and disk management. The data acquired by the data acquisition module are temporarily stored on the hard disk of the CompactRIO real-time controller. To ensure the security and stability of the system, the disk of the real-time controller is encrypted and cannot be accessed by ordinary users. Therefore, an automatic disk management function was developed for file management. To prevent the loss of data files, they are automatically sent to the hard disk of the ACS via FTP protocol before the running of the file management process. During the file deletion process, files in a specific folder are sorted in chronological order of their creation, and the oldest file is deleted first. Therefore, the beam diagnostic electronic system can save recent files without filling the entire disk.

The initialization function is used to initialize all procedures and underlying devices. In addition, an error handling function was designed for error monitoring and tracking on the beam diagnostic electronics system. Thus, the operation and maintenance personnel can quickly find the location of faults. The error handling function was developed based on the NI Fault Engine in the scan engine of CompactRIO. In the case of an error, the appropriate measures are implemented for the beam diagnostic electronics system according to the severity of the error.

For the convenient maintenance and traceability of the operation of the beam diagnostic electronics system by the operating personnel and for the localization of the origin of failures for maintenance engineers, the beam diagnostic electronics system is equipped with a log recording function, which records all instruction operations and error information. The function of recording instruction operations includes the record of the time and all instructions sent from the ACS. This function ensures the traceability of operations performed by the operating personnel. The error information recording function records the time, location, and error codes of the errors occurred in the scan engine of the real-time controller, which enables maintenance personnel to find the origin of failures quickly.

The watchdog module automatically restores the system to the normal working state when the system crashes due to potential program errors and harsh environmental interference. The heartbeat module informs the users if the connection between the electronics system and the ACS is operational and the electronics system is running normally.

A queue message handler (QMH) design pattern was used to satisfy the requirements of communication within one process and between different processes to realize data acquisition, motion control, status uploading, error processing, and log recording. The QMH design pattern was designed to receive, store, and process messages, which was implemented based on the asynchronous message communication (AMC) library. The QMH design pattern was modified to run on the CompactRIO controller, based on a Linux system. In the modified QMH design pattern, messages from the generators are stored in message queues and are read by the processors. The message processor is composed of multiple cases or states, and each is dedicated to processing a specific message or multiple messages.

In the beam diagnostic electronics system, all procedures are implemented using the modified QMH design pattern. A message queue with a specific name is created for each module. For each message queue, the message processor is composed of multiple cases. Different cases are designed to implement different operations, such as processing messages from other message queues and sending messages to itself or other message queues.

The functions of the main module of the beam diagnostic electronics system include sending system initialization messages to other message queues, uploading initialization state messages to the OPC UA module, and recording and uploading error information. Different functions are implemented in different cases of the modified QMH design pattern.

3 Testing and calibration

The beam diagnostic system operates in a complex electromagnetic environment. Several interference factors, such as magnetic coupling and electromagnetic radiation interferences, have noticeable influence on the accuracy of the measurement unit. Moreover, the analog voltage signal outputs by the picoammeters are also coupled to a large number of higher harmonics, rather than being fully proportional to the corresponding current signals. Therefore, to improve the accuracy of the measurement unit, testing and calibration procedures are required.

To generate reference current signals for the measurement unit, a high-precision current source was used. In the test, the current signal was fed into the probe, converted to a voltage signal by the picoammeter, and then sampled by the data acquisition card. The resolutions of the current source and picoammeters were 6.5 and 5.5 digits, respectively; both of them were calibrated at the metrology institute.

For different picoammeter ranges from 2 nA to 2 μA, the reference signals were set to the corresponding half range, and for each range 200,000 measurements were chosen. The characteristics of the measurement unit were analyzed based on the frequency distributions of the measured values. Figure 4a shows the histogram of the measured values in the 2-nA and 20-nA ranges. The interval widths of the histogram are 0.01 and 0.001 V, respectively. It can be seen that the frequency distributions of the measured values follow a normal distribution. The mean and root mean square (RMS) of the measured values were obtained from a Gaussian fitting. This indicates that compared with those in the 20 nA range, the random and systematic errors in the 2 nA range are both larger. In addition, similar patterns were observed from the measured values in the 200 nA and 2 μA ranges.

Based on the analysis of the mean measured values in different ranges, it was observed that there was a certain measurement bias between the mean measured values and corresponding reference values. To verify the linearity of the measurement unit, the current signal output by the current source was varied in the range of 10–100% for each range as reference values for different ranges from 2 nA to 2 μA. The mean measured values were also obtained by a Gaussian fitting as mentioned above.

According to the distributions of the mean measured values, a linear fitting between the mean measured values and reference values was performed, as shown in Fig. 4b.

As can be seen in Fig. 4b, there is a high degree of linearity between the mean measured values and reference values, indicating that the measurement biases are predictable and can be considered as systematic measurement errors. Therefore, the measured values can be corrected using linear fitting equations.

The linearity of the measurement unit was verified according to the above experimental and analytical results. However, these experiments only considered the characteristics of the measurement unit. It should be noted that the interference from the RF system strongly affects the measurement accuracy of the beam intensity as well. To explore the effect of the RF system on the measurement unit of the MRBDS and to develop a calibration scheme to improve its measurement accuracy, the background noise was measured under the stable operation of the RF system and the superconducting magnet system. During the operation, the train probe moved outward from the central region to the extraction region of the cyclotron with a step size of 1 mm. For each measurement point, 2000 repeated tests were performed. The frequency distribution of the measured values indicates that the measured values at each measurement point follow a Gaussian distribution based on the Kolmogorov–Smirnov test [18, 19]. Therefore, the expectation and standard deviation values of the background noise can be obtained by Gaussian fitting. The experimental results at 12 key positions are shown in Fig. 5.

As can be seen in Fig. 5, the electromagnetic noise from the RF system mainly depends on the position of the train

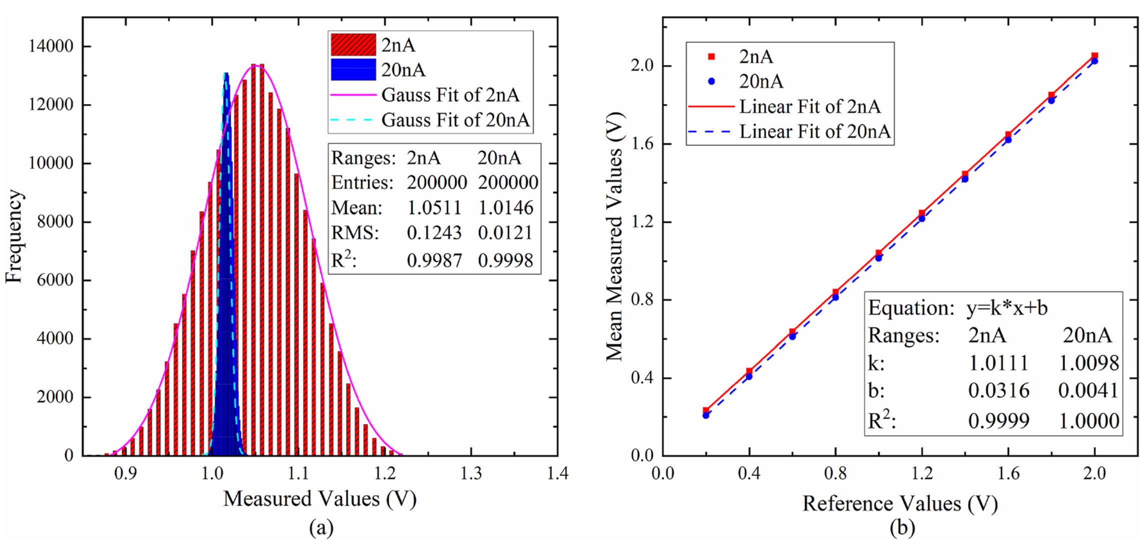

Fig. 4 (Color online) **a** Frequency distribution of the output values of the picoammeter in the 2-nA and 20-nA ranges. **b** Linear fitting between the mean measured values and the reference values

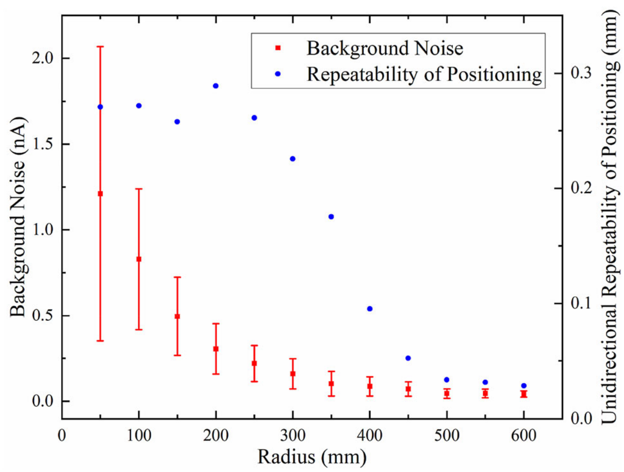

Fig. 5 (Color online) Background noise and unidirectional repeatability of positioning as functions of radius

probe. The closer it is to the central region, the stronger the background noise is. Therefore, the accuracy of the measurement unit can be significantly improved by subtracting the corresponding background noise. It should be noted that when the output power of the RF system strongly fluctuates, the background noise increases sharply. These measurement data were discarded.

The positioning accuracy of the train probe also has a noticeable effect on the beam diagnosis. Therefore, the repeatability of the probe needs to be as good as possible, which is affected by factors such as the characteristics of the transmission mechanism, time delay, and the stiffness of the electronics system.

The curved guide rail consists of a straight section and two tangent arc sections. As the train probe moves along the curved guide rail, the repeatability of the positioning needs to be determined is three dimensions. In the experiment, five points were selected in the straight section, and seven points were selected in the arc sections as reference points. Five repeated tests were performed for each reference point to determine the repeatability of the positioning of the train probe. A laser tracker was used to measure the three-dimensional coordinates of the probe, and an auxiliary tool mounted temporarily on the probe was designed to position the target of the laser tracker.

According to ISO 230-2:2014 standard [20] and the characteristics of the train probe, the definition of the estimator of the unidirectional standard uncertainty of positioning at position P_i can be modified as

$$S_i = \sqrt{\frac{1}{n-1}\sum_{j=1}^{n}\left[\left(X_{ij}-\bar{x}_i\right)^2+\left(Y_{ij}-\bar{y}_i\right)^2+\left(Z_{ij}-\bar{z}_i\right)^2\right]}, \tag{1}$$

where S_i denotes the estimator of the unidirectional standard uncertainty of positioning at position P_i, n is the number of unidirectional approaching experiments, X_{ij}, Y_{ij}, and Z_{ij} are deviations in position in the X, Y, and Z directions of the jth experiment, respectively, and $\bar{x}_i$, $\bar{y}_i$, and $\bar{z}_i$ represent the mean unidirectional positional deviations in the three coordinate directions at position P_i of n experiments. The unidirectional repeatability R_i of positioning at position P_i is defined as the range obtained from the expanded uncertainty of unidirectional positional deviations at position P_i using a coverage factor of 2 as

$$R_i = 4S_i. \tag{2}$$

According to the measurement data from the laser tracker and the calculations using Eqs. (1) and (2), the calculated results of the unidirectional repeatability of positioning at 12 reference points are also shown in Fig. 5. The first seven points are located in the arc sections, while the others are located in the straight section.

As can be seen in Fig. 5, the unidirectional repeatability of positioning of the probe in the straight section is less than 0.1 mm, while the unidirectional repeatability of positioning at the arc sections is noticeable higher. The unidirectional repeatability of positioning is close to 0.3 mm when the probe is at the small radius of the cyclotron. The unidirectional repeatability of the positioning of the train probe was proven to satisfy the requirements of beam diagnosis proposed by the designers and verified by practical tests. Additionally, extensive tests indicate that the unidirectional repeatability of the positioning of the train probe needs to be verified monthly. Moreover, the eccentric bolts can effectively and easily prevent the degradation of repeatability of the train probe.

4 Commissioning and discussion

During beam commissioning, the MRBDS was used to determine the optimum parameters, such as the frequency of the RF system, main coil current, installation angle, and height of the ion source, by measuring the beam intensities at different radii of the cyclotron. In addition, the MRBDS can also determine the radius of the beam loss.

To further prove the efficiency and applicability of the train probe, the MRBDS was used to measure the phase lag of the particles in the beam according to the Smith–Garren method [21, 22]. Furthermore, the measurement results were compared with the calculated theoretical results. The phase lag at radius R for particles in the beam is given by

$$\sin\varphi(R) \approx \sin\varphi(0) - \frac{2\pi m\omega^2}{\Delta E}\left(\int_0^R \frac{\Delta B(r)}{B_s(0)} r\mathrm{d}r - \frac{\Delta\omega}{\omega}\frac{R^2}{2}\right), \tag{3}$$

where $\Delta B(r)$ is the difference between the actual magnetic field at radius r and the synchronous field $B_s(r)$ corresponding to frequency ω, ΔE denotes the peak energy gain per turn, and m denotes the mass of the particle. The last term on the right can be ignored because the frequency ω is kept constant for the isochronous cyclotron.

According to Eq. (3), the phase lag is a function of the main magnetic field. In the process of beam diagnosis, the most convenient method for varying the main magnetic field is to adjust the main coil current. Therefore, the phase lag is a function of the main coil current [23] and given by

$$\sin\varphi(R) = 2\frac{\bar{I} - I_0}{\Delta I}, \tag{4}$$

where $\bar{I} = [I^-(R) + I^+(R)]/2$, $\Delta I = I^-(R) - I^+(R)$, $I^-(R)$, and $I^+(R)$ correspond to the main coil current when the phase lag at radius R is equal to $-90°$ and $+90°$, respectively. It should be noted that when the phase lag at radius R exceeds $\pm 90°$, the beam is lost completely, and the measured beam intensity becomes zero. The value of I_0 corresponds to the main coil current when the measured beam intensity at the extraction radius is the highest.

A set of curves of beam intensities measured by the MRBDS at different radii is shown in Fig. 6 as functions of the main coil current. For each curve, the main coil currents corresponding to half of the maximum beam intensity value are taken as $I^+(R)$ and $I^-(R)$, respectively, considering that it is difficult to determine the corresponding main coil current when the beam intensity is zero from Fig. 6. Moreover, I_0 represents the main coil current when the beam intensity reaches a maximum at a radius of 550 mm.

The phase lag values at different radii can be obtained using Eq. (4) from the data shown in Fig. 6. A comparison of the phase lag values of the particles in the beam measured by the MRBDS and the theoretical values of the phase lag calculated using orbit tracking is shown in Fig. 7. As can be seen in Fig. 7, the measurement results of the phase lag with respect to the radius are very close to the theoretical results, which prove the suitability of the MRBDS.

To assess the cumulative measurement errors of the MRDBS, the expanded uncertainties were calculated, which are shown in Fig. 7 as error bars. The uncertainty $u(m)$ introduced by the measurement unit, the uncertainty $u(p)$ of the measured values resulting from the positioning error of the transmission unit, and the uncertainty $u(I_0)$ due to temperature variations during the measurement were considered in the calculation of the combined standard uncertainty $u_c(y)$. The expanded uncertainty $U(y)$ can be calculated as

$$U(y) = ku_c(y) = k\sqrt{u^2(m) + u^2(p) + u^2(I_0)}, \tag{5}$$

where a coverage factor of $k = 2$ was used.

According to Eq. (4), the measured value of the phase lag is a function of the radius and the main coil current. The functional relation $f(I_B)$ between the main coil current and the measured beam current can be determined using the test results shown in Fig. 6. Thus, the uncertainty $u(m)$ at the specified radius introduced by the measurement unit can be calculated using the law of the propagation of uncertainties as

$$u(m) = \left|\frac{\partial[\sin\varphi(R)]}{\partial I^-}\right| u(I^-) + \left|\frac{\partial[\sin\varphi(R)]}{\partial I^+}\right| u(I^+), \tag{6}$$

$$u(I^-) = u(I^+) = \left|\frac{\partial[f(I_B)]}{\partial I_B}\right| u(I_B), \tag{7}$$

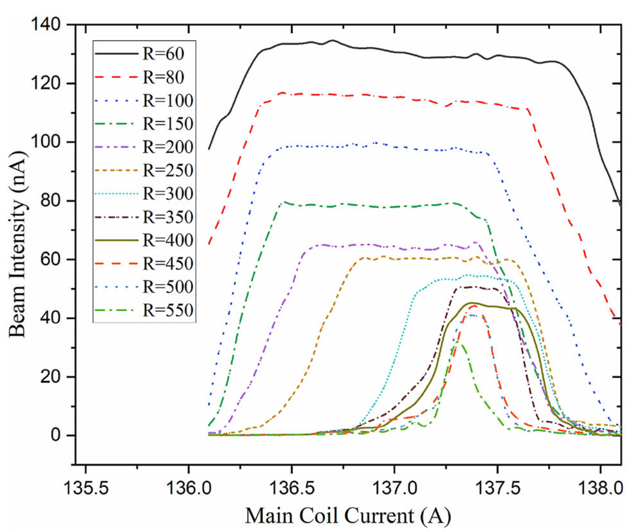

Fig. 6 (Color online) Beam intensities for different main coil current values measured by the MRBDS at radii ranging from 60 to 550 mm

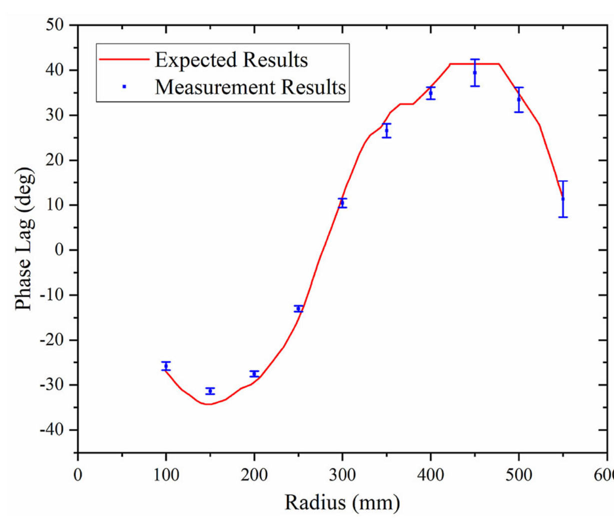

Fig. 7 Comparison of the phase lag results measured by the MRBDS and the theoretical results calculated using orbit tracking

where $u(I^-)$ and $u(I^+)$ are the standard uncertainties of the main coil current, I_B is the measured beam current, and $u(I_B)$ is determined by a type A evaluation method, which is the standard deviation of the arithmetic mean of the measured beam current in the 200-nA range.

As shown in Fig. 7, the theoretical value of the phase lag is a function of the radius, whose functional expression $h(R)$ can be calculated using orbit tracking. Therefore, uncertainty $u(p)$ can be calculated as

$$u(p) = \left|\frac{\partial h(R)}{\partial R}\right| u(R), \tag{8}$$

where $u(R) = S_i$ is given by Eq. (1). Similarly, the phase lag at the specified radius is also a function of I_0. Thus, the uncertainty $u(I_0)$ is given by

$$u(I_0) = \left|\frac{\partial[\sin\varphi(R)]}{\partial I_0}\right| u(\Delta I_0). \tag{9}$$

where the estimated uncertainty of $u(\Delta I_0)$ is $\pm$ 3 mA due to temperature variations during the measurement.

5 Conclusion

A main radial beam diagnostic system equipped with a new type of train probe is developed to achieve high-precision beam diagnosis for the SC200 superconducting cyclotron. In this paper, the detailed design of the mechanical structure and electronics system is presented. Calibration experiments were conducted to demonstrate the linearity of the measurement unit. In addition, the background noise was measured under the stable operation of the RF system, and the calibration of the measurement unit was performed accordingly. Furthermore, the repeatability test of the transmission mechanism indicated that the unidirectional repeatability of the positioning was better than 0.3 mm, which was proven to satisfy the requirements of beam diagnosis in practical applications.

Finally, the phase lag curves of the particles in the beam were measured by the MRBDS, and the results were compared with the theoretical values, which proved the efficiency and applicability of the MRBDS.

The MRBDS was manufactured, assembled, and calibrated. Functional and stability tests were also implemented, which indicated that the train probe was an effective solution, which can be extended for the measurement in confined spaces or vacuum environments.

References

1. W.Q. Chen, R.S. Zheng, P.D. Baade et al., Cancer statistics in China. CA A Cancer J. Clin. **66**, 115–132 (2016). https://doi.org/10.3322/caac.21338
2. R.A. Amos, Proton and carbon ion therapy. Med. Phys. (2013). https://doi.org/10.1118/1.4802213
3. J.E. Munzenrider, N.J. Liebsch, Proton therapy for tumors of the skull base. Strahlenther. Onkol. **175**, 57–63 (1999). https://doi.org/10.1007/978-1-4614-5298-0_8
4. K.Z. Ding, Y.F. Bi, G. Chen et al., Study of the beam extraction from superconducting cyclotron SC200. Cyclotr. Appl. (2016). https://doi.org/10.18429/jacow-cyclotrons2016-mop14
5. M.M. Xu, Y.T. Song, G. Chen et al., Design and commissioning of Brav measurement system for SC200 superconducting cyclotron. Nucl. Sci. Tech. **30**, 93 (2019). https://doi.org/10.1007/s41365-019-0614-2
6. F. Jiang, Y.T. Song, J.X. Zheng et al., Energy loss of degrader in SC200 proton therapy facility. Nucl. Sci. Tech. **30**, 4 (2019). https://doi.org/10.1007/s41365-018-0526-6
7. G.A. Karamysheva, O.V. Karamyshev, N.A. Morozov et al., Magnetic system for SC200 superconducting cyclotron for proton therapy, in Proceedings of the 13th International Conference on Cyclotrons and Their Applications, pp 353–355 (2016). https://doi.org/10.18429/jacow-cyclotrons2016-thc03
8. M. Olivo, Beam diagnostic equipment for cyclotrons, in Seventh International Conference on Cyclotrons and their Applications, pp. 331–340 (1975). https://doi.org/10.1007/978-3-0348-5520-4_70
9. P. Strehl, Beam Instrumentation and Diagnostics. Springer, Berlin. (2006). https://doi.org/10.1007/3-540-26404-3
10. F.P. Guan, H. Xie, L. Wen et al., The development of radial probe for CYCIAE-100, in Proceedings of the International Conference on Cyclotrons and Their Applications, pp. 165–167 (2013). https://accelconf.web.cern.ch/CYCLOTRONS2013/papers/tuppt006.pdf
11. T.J. Zhang, H.J. Yao, Z.G. Li et al., Physical problems and beam test of compact cyclotron. High Power Laser Particle Beams **25**, 104–108 (2013). https://doi.org/10.3788/HPLPB20132501.0104. **(in Chinese)**
12. L. Rezzonico, Beam diagnostics at sin, in 7th International Conference on Cyclotrons and Their Applications, I5-05, pp. 457–460 (1987). http://accelconf.web.cern.ch/c86/papers/i505.pdf
13. S. Roy, S. Bhattacharya, T. Das et al., Beam Diagnostic components for superconducting cyclotron at Kolkata, in Proceedings of the 19th ICCA, Lanzhou, pp. 102–104 (2010). https://doi.org/10.18429/jacow-cyclotrons2010-MOPCP091
14. E. Acerbi, G. Raia, G.C. Rivoltella et al., The Beam diagnostics of the Milan K800 cyclotron, in Proceedings of the 12th ICCA, pp. 283–286 (1989). https://accelconf.web.cern.ch/c89/papers/f5-03.pdf
15. L. Calabretta, G. Cuttone, S. Gammino et al., Commissioning of the K800 INFN cyclotron, in Proceedings of the 14th ICCA, pp. 12–19 (1996). https://www.researchgate.net/publiccation/236626569
16. P.Y. Zhou, Y.T. Song, K.Z. Ding et al., Research on the method of magnetic field shimming for superconducting cyclotron. Nucl. Tech. **42**, 030201 (2019). https://doi.org/10.11889/j.0253-3219.2019.hjs.42.030201. **(in Chinese)**
17. D. Bruckner, M.P. Stanica, R. Blair et al., An introduction to OPC UA TSN for industrial communication systems, in Proceedings of the IEEE, pp. 1121–1131 (2019). https://doi.org/10.1109/JPROC.2018.2888703

18. N. Smirnov, Table for estimating the goodness of fit of empirical distributions. Ann. Math. Stat. **19**, 279–281 (1948). https://doi.org/10.1214/aoms/1177730256
19. J. Frank, The Kolmogorov–Smirnov test for goodness of fit. J. Am. Stat. Assoc. **46**, 68–78 (1951). https://doi.org/10.1080/01621459.1951.10500769
20. ISO 230-2: 2014, Test code for machine tools—part 2: determination of accuracy and repeatability of positioning of numerically controlled axes, an international organization for standardization (2014). https://www.iso.org/standard/55295.html
21. A.A. Garren, L. Smith, Diagnosis and correction of beam behaviour in an isochronous cyclotron, in Proceedings of the International Conference on Sector-Focused Cyclotrons and Meson Factories (1963). https://doi.org/10.18429/jacow-cyclotrons1963-CYC63A03
22. K. Daniel, K. Gugula, J. Sulikowski et al., Operation mode of AIC-144 multipurpose isochronous cyclotron for eye melanoma treatment, in Proceedings of Cyclotrons 2013, pp. 461–463 (2013). https://accelconf.web.cern.ch/CYCLOTRONS2013/papers/fr1pb01.pdf
23. C. Baumgarten, A. Geisler, U. Klein et al., Isochronism of the ACCEL 250 MeV medical proton cyclotron. Nucl. Instrum. Methods B **570**, 10–14 (2007). https://doi.org/10.1016/j.nima.2006.09.112